Available online at www.sciencedirect.com

ScienceDirect

journal homepage: www.elsevier.com/locate/he

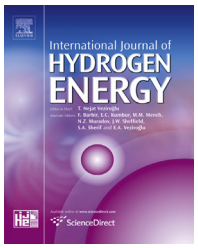

Aqueous phase reforming of sorbitol on Pt/Al_2O_3: Effect of metal loading and reaction conditions on H_2 productivity

H.A. Duarte, M.E. Sad, C.R. Apesteguía *

Catalysis Science and Engineering Research Group (GICIC), INCAPE, UNL-CONICET, Predio CCT Conicet, Paraje El Pozo, 3000 Santa Fe, Argentina[1]

ARTICLE INFO

Article history:
Received 20 April 2016
Received in revised form
28 June 2016
Accepted 11 July 2016

Keywords:
Aqueous-phase reforming
Sorbitol
H_2 production
Pt/Al_2O_3 catalysts
Green chemistry

ABSTRACT

The production of hydrogen by aqueous phase reforming (APR) of sorbitol was studied on Pt-based catalysts at 498 K and 29.3 bar. Four alumina-supported Pt catalysts (0.30, 0.57, 1.50 and 2.77%wt Pt) were prepared. The influence of both the metallic content and the weight hourly space velocity (WHSV, h^{-1}) on sorbitol conversion and hydrogen selectivity, yield and productivity was investigated. Sorbitol conversion and H_2 yield increased with the amount of Pt while the H_2 selectivity in the gas phase did not change significantly. The H_2 productivity was measured on all the catalysts at different WHSV in order to determine the operating conditions required to optimize the production of hydrogen. The H_2 productivity increased with the amount of Pt and went through a maximum as the space velocity was increased. The highest H_2 productivity (22 mmol H_2/h g_{cat}) was achieved on $Pt(2.77\%)/Al_2O_3$ at WHSV = 1.8 h^{-1}. At a given space velocity, the H_2 productivity did not depend on the sorbitol concentration in the feed.

Introduction

Aqueous Phase Reforming (APR) is a promising technology for producing hydrogen from biomass-derived compounds such as ethylene glycol, glycerol, sugars, and sugar alcohols [1–5]. The APR of these polyols is a CO_2 neutral process to generate hydrogen in a single step at moderate temperatures (between 423 K and 543 K) where the water-gas shift reaction (WGS) is favorable, thereby producing only traces of carbon monoxide. Also, the APR process eliminates the need to volatilize water which results in a higher energy efficiency compared to vapor-phase steam-reforming processes [6]. Production of H_2 from APR process was initially studied using mainly ethylene glycol and glycerol as substrates [7–10]. More recently, several papers have investigated the liquid phase processing of sorbitol, a sugar alcohol obtained by hydrogenation of glucose, that presents a more complicated process chemistry of APR than ethylene glycol or glycerol [11–15]. Fig. 1 shows a simplified scheme of the reaction network for APR of sorbitol, based on the main reaction pathways that would take place on metal/acid bifunctional catalysts, according to previous work [16,17]. The stoichiometric formation of hydrogen via APR of sorbitol is represented by endothermic reaction 1 (ΔH = 230 kJ/mol):

$$C_6O_6H_{14} + 6\,H_2O \rightarrow 6\,CO_2 + 13\,H_2 \quad (1)$$

* *Corresponding author.*
E-mail address: capesteg@fiq.unl.edu.ar (C.R. Apesteguía).
[1] *URL:* http://www.fiq.unl.edu.ar/gicic

http://dx.doi.org/10.1016/j.ijhydene.2016.07.071
0360-3199/

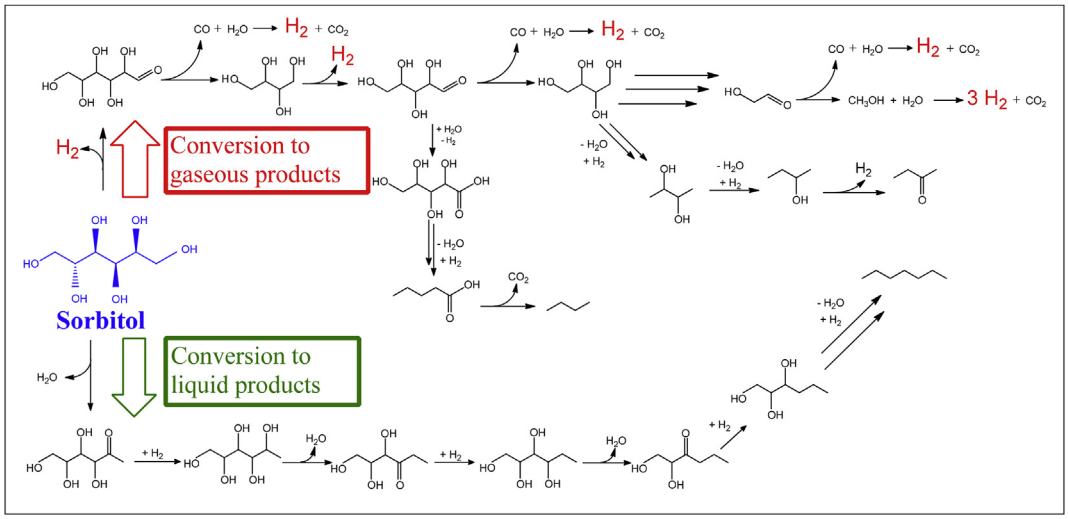

Fig. 1 – Reaction network of the APR of sorbitol.

Other reactions that may simultaneously form H_2 are the endothermic decomposition of sorbitol (reaction 2) and the exothermic water gas shift reaction (reaction 3)

$$C_6O_6H_{14} \rightarrow 6\,CO + 7\,H_2 \quad (2)$$

$$CO + H_2O \rightarrow CO_2 + H_2 \quad (3)$$

Exothermic methanation of CO and CO_2 (reactions 4 and 5) may also take place:

$$CO + 3\,H_2 \rightarrow CH_4 + H_2O \quad (4)$$

$$CO_2 + 4\,H_2 \rightarrow CH_4 + 2\,H_2O \quad (5)$$

Overall, the selectivity of the reactions involved in APR of sorbitol as depicted in Fig. 1 may be adjusted to produce gaseous H_2 (by promoting the C–C bond cleavage reactions) or liquid alkanes and oxygenates (by promoting C–O bond hydrogenolysis reactions while preserving C–C bonds). Catalysts will play then a major role to promote the desired reaction pathways for sorbitol processing, although other factors such as concentration of sorbitol feedstock, space velocity, and reaction temperature and pressure, may also greatly influence the final product distribution. The production of hydrogen by APR of sorbitol has been studied mainly on Pt supported on alumina or carbon [1,11,12,14–16,18], probably because Pt is more selective for H_2 production than other noble metals [19] and alumina or carbon do not contain strong surface acid sites that promote sorbitol conversion to liquid products [20]. The development of competing technology for generating hydrogen from biomass requires the use of highly active, selective and cost-effective catalysts for achieving optimal H_2 productivity. Due to the high cost and limited availability of Pt, it is significant to stablish what is the minimum Pt loading required to obtain active, selective and stable catalysts for achieving the highest H_2 productivity. Nevertheless, studies addressing the relationship between the Pt loading and the H_2 productivity for sorbitol processing on Pt-supported catalysts are still lacking. Precisely, in this work we investigate the APR of sorbitol on Pt/Al_2O_3 catalysts containing different amounts of platinum. The aim was to stablish the effect of Pt loading and weight hourly space velocity on hydrogen selectivity, yield and productivity.

Experimental

Catalyst preparation and characterization

Four Pt/Al_2O_3 catalysts of different Pt loadings (0.30, 0.57, 1.50 and 2.77%wt) were prepared by incipient wetness impregnation at 303 K of a high-purity γ-Al_2O_3 powder (Cyanamid Ketjen CK300, 220 m^2/g, 0.49 cm^3/g pore volume) with an aqueous solution of tetraamine platinum nitrate, $Pt(NH_3)_4(NO_3)_2$ (Aldrich, 99.99%). The impregnated samples were dried overnight at 353 K, then heated in air at 773 K for 3 h and finally reduced 2 h at 773 K in pure hydrogen.

BET surface areas (S_{BET}) were measured by N_2 physisorption at 77 K in a Autosorb Quantochrome Instrument 1-C sorptometer. Pt loadings were measured by inductively coupled plasma atomic emission spectroscopy (ICP-AES), using a Perkin–Elmer Optima 2100 unit. The Pt dispersion (D_{Pt}, surface Pt atoms/total Pt atoms) of the samples was determined by chemisorption of hydrogen. Volumetric adsorption experiments were performed at 298 K in a conventional vacuum unit. Catalysts were reduced in H_2 at 573 K for 2 h and then outgassed 2 h at 773 K prior to performing gas chemisorption experiments. Hydrogen uptake was determined using the double isotherm method as detailed elsewhere [21]. A stoichiometric atomic ratio of $H/Pt_s = 1$, where Pt_s implies a Pt atom on surface, was used to calculate the metal dispersion. Powder X-ray diffraction (XRD) patterns were collected in the range of $2\theta = 10–70^\circ$ using a Shimadzu XD-D1 diffractometer and Ni-filtered Cu K_ϵ radiation.

Acid site densities were determined by using temperature-programmed desorption (TPD) of NH_3 preadsorbed at 373 K. Samples (200 mg) were treated in He (60 cm^3/min) at 773 K for

1.5 h, cooled down to 373 K and exposed to a 1% NH_3/He stream until surface saturation. Weakly adsorbed NH_3 was removed by flushing with He at 373 K for 0.5 h. Temperature was then increased at 10 K/min and the NH_3 concentration in the effluent was measured by mass spectrometry (MS) in a Baltzers Omnistar unit.

The nature of surface acid sites on alumina was determined by infrared spectroscopy (IR) in a Shimadzu FTIR Prestige-21spectrophotometer using pyridine as probe molecule. Samples were ground to a fine powder and pressed into wafers (10–30 mg). The discs were mounted in a quartz sample holder and transferred to an inverted T-shaped Pyrex cell equipped with CaF_2 windows. Samples were initially outgassed in vacuum at 723 K during 2 h and then a background spectrum was recorded after being cooled down to room temperature. Spectra were recorded at room temperature, after admission of pyridine, and sequential evacuation at 303, and 373 K.

Catalytic testing

The APR of sorbitol was carried out in a fixed-bed flow reactor at 498 K and 29.3 bar. Samples were sieved to retain particles with 0.35–0.42 mm diameter for catalytic measurements and treated in-situ at 573 K with pure H_2 (75 cm^3/min) for 1 h before reaction. The aqueous solution containing 1%wt sorbitol (Sigma Aldrich, 99.9%) was introduced to the reactor in a N_2 carrier flow (20 cm^3/h STP) using a HPLC-type pump (Alltech 310). The flow rate of liquid was varied between 6 ml/h and 24 ml/h. The reactor effluent was cooled down by passing through a condensation system and then conducted to a gas–liquid separator. The gas products were analyzed on line in a Shimadzu GC-2014 gas chromatograph equipped with a Hayesep D 100–120 column (5 m × 1/8 in × 2.1 mm), and thermal conductivity (TCD) and flame ionization (FID) detectors. Hydrogen was quantified using the TCD detector while CO, CO_2 and CH_4 were analyzed by FID after completely converting CO and CO_2 to methane by means of a methanation catalyst (Ni/Kieselghur) operating at 673 K. Condensable products were drained periodically and quantified by using high-performance liquid chromatography (HPLC) in a UFLC Shimadzu LC chromatograph equipped with a BioRad Aminex HPX-87C column (250 × 4.0 mm) and a refraction index detector (RID).

The total conversion of sorbitol (X_S) to gaseous and liquid products was calculated as:

$$X_S = \frac{F_S^0 - F_S}{F_S^0}$$

where F_S^0 and F_S are the sorbitol molar flow at the inlet and the exit of the reactor, respectively. The carbon-based conversion of sorbitol to gaseous products is:

$$X_S^G = \frac{\sum \alpha_i F_i}{\alpha_S F_S^0}$$

where α_i are the number of C atoms in the product i molecule, F_i is the molar flow of gaseous product i formed from sorbitol, and α_S are the number of C atoms in the sorbitol molecule. In our case, the C-containing gaseous products formed from sorbitol were CO, CO_2 and CH_4, so that X_S^G becomes:

$$X_S^G = \frac{F_{CO} + F_{CH_4} + F_{CO_2}}{6\,F_S^0}$$

The conversion of sorbitol to liquid products, X_S^L, was calculated as the difference between X_S and X_S^G. The yield to H_2 (η_{H_2}, moles of H_2 produced/moles of sorbitol fed) was calculated by taking into account the stoichiometric factors of Reaction 1:

$$\eta_{H_2} = \frac{F_{H_2}}{F_S^0} \cdot \frac{1}{13}$$

The selectivity to H_2 in the gas phase (S_{H_2}, molecules H_2 produced/C atoms in gas phase), was determined as:

$$S_{H_2} = \frac{F_{H_2}}{F_{CO} + F_{CO_2} + F_{CH_4}} \cdot \frac{1}{RR}$$

where RR, the H_2/CO_2 reforming ratio, is 13/6 and represents the maximum H_2/C molar ratio that can be obtained according to the stoichiometry of reaction 1. Finally, the H_2 productivity (Pr, mol H_2/h g_{cat}) was calculated as $Pr = \frac{F_{H_2}}{W_{cat}}$.

Results and discussion

Catalyst characterization

The density of surface acid sites of commercial Al_2O_3 CK300 used in this work was determined by TPD of NH_3 preadsorbed at 373 K. By integration of TPD curves (not shown here) we obtained a value of 3.2 mmol NH_3/g, which is comparable to those reported in literature for similar alumina supports [22,23]. The nature of Al_2O_3 surface acid sites was established from the FTIR spectra of adsorbed pyridine. Fig. 2 shows the spectra obtained after admission of pyridine, adsorption at room temperature, and sequential evacuation at 303 and 373 K. The pyridine absorption bands at around 1540 cm^{-1} and 1450 cm^{-1} arise from pyridine adsorbed on Brønsted and

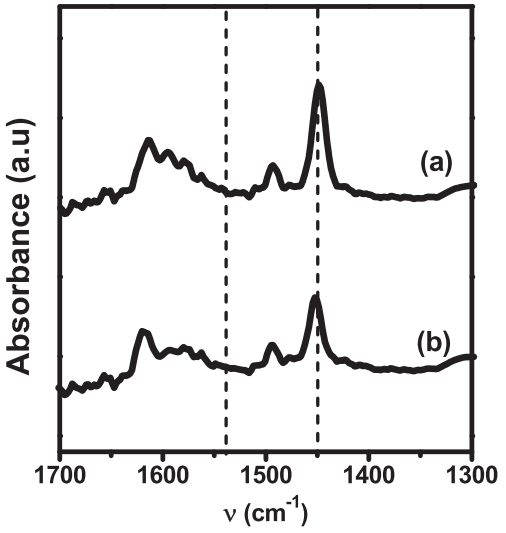

Fig. 2 – FTIR spectra of pyridine adsorbed at 298 K and evacuated at 303 K (a) and 373 K (b) on Al_2O_3.

Lewis acid sites, respectively. The IR spectra of Fig. 2 show that Al_2O_3 CK300 contains essentially Lewis acid sites.

XRD diffractograms of Al_2O_3, Pt(1.50)/Al_2O_3 and Pt(2.77)/Al_2O_3 are presented in Fig. 3. The XRD patterns exhibited only the alumina crystalline structure of the support, thereby suggesting that Pt was well dispersed on the support. The Pt loading, surface area and metal dispersion of Pt/Al_2O_3 catalysts are given in Table 1. The BET surface area of Al_2O_3 CK300 (220 m^2/g) did not change significantly after the metal impregnation and the consecutive oxidation/reduction steps used for obtaining Pt/Al_2O_3 catalysts. The Pt dispersion decreased slightly with the metal loading, from 67% on Pt(0.30)/Al_2O_3) to 54% on Pt(2.77)/Al_2O_3

Catalytic results

Fig. 4 shows the evolution of sorbitol conversions (X_S, X_S^G , X_S^L) and H_2 selectivity (S_{H_2}) as a function of time at a space velocity (WHSV, $g_{sorbitol}/g_{cat}$ h) of 1.2 h^{-1} for the four Pt catalysts used in this work. In all the cases, the start-up of the reaction required about 2 h to obtain stationary values of sorbitol conversions and H_2 selectivity. In Table 2 we present the results obtained at the end of the runs when varying WHSV from 0.6 h^{-1} to 2.4 h^{-1}. The H_2 yield values (η_{H_2}) are also included in Table 2.

Data in Fig. 4 and Table 2 show that at WHSV = 1.2 h^{-1} the total conversion of sorbitol increased with the Pt loading on the catalyst, from 36% (0.30% Pt) to 61% (2.77% Pt); similarly, X_S^G increased from 12% to 27% and X_S^L from 24% to 34%. The H_2 yield also increased with % Pt while S_{H_2} did not change significantly. A similar qualitative trend between the activity/selectivity parameters (X_S^G, X_S^L, S_{H_2}) and Pt loading was observed when the reaction was carried out at different WHSV values (Table 2). These results show that the Pt loading increase essentially improves the catalyst activity, probably reflecting the concomitant generation of surface metallic active sites. In this regard, we have represented in Fig. 5 the evolution of sorbitol conversion to gaseous products (X_S^G) as a function of the amount of surface Pt fraction (Pt_s, μmol Pt/g_{cat}) determined using the metallic dispersion values of Table 1. Fig. 5 shows that for a given WHSV value, X_S^G increased continuously but not linearly with Pt_s; comparatively, the effect of Pt_s on sorbitol conversion was more important in the lower Pt_s region. For example, at WHSV = 0.6 h^{-1} X_S^G increased from 21% to 30% by increasing Pt_s from 10.3% to 18.4%, respectively, while X_S^G increased only from 37% to 39% when Pt_s was increased from 43.1% to 76.7%.

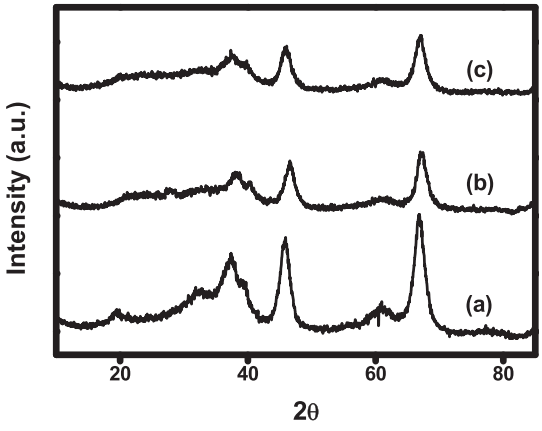

Fig. 3 – XRD diffractograms of: (a) Al_2O_3; (b) Pt(1.50)/Al_2O_3; (c) Pt(2.77)/Al_2O_3.

Table 1 – Catalyst properties.

Catalyst	Pt loading (%)	S_{BET} (m^2/g)	D_{Pt} (%)
Pt(0.3)/Al_2O_3	0.30	217	67
Pt(0.57)/Al_2O_3	0.57	223	63
Pt(1.5)/Al_2O_3	1.50	206	56
Pt(2.77)/Al_2O_3	2.77	209	54

In contrast with catalyst activity, the selectivity to H_2 did not change significantly with the Pt loading (Table 2). In Table 3 we present the product distribution in the gas phase obtained on Pt(0.30)/Al_2O_3 and Pt(2.77)/Al_2O_3 catalysts. Similar quantitative product distribution was observed on both samples at the space velocities studied in this work: 60–70% H_2, 27–36% CO_2, 3–5% CH_4, and traces of CO. The amount of C_2–C_6 hydrocarbons in the gas phase was lower than 1% in all the cases, which is consistent with results reported in previous work on APR of sorbitol [1,16] when no hydrogen is fed to the reactor, as is the case here.

The stoichiometric gas composition to be obtained from the APR of sorbitol according to reaction 1 is 68.4% H_2 and 31.6% CO_2. In summary, the results of Table 3 shows that the gaseous product distribution for the APR of sorbitol on Pt/Al_2O_3 catalysts does not depend significantly on the Pt loading, the Pt crystallite size or the sorbitol conversion level.

As expected, the sorbitol conversion diminished with space velocity (Table 2). For example, on Pt(1.50)/Al_2O_3 sorbitol conversions at WHSV = 0.6 h^{-1} were X_S = 84%, X_S^G = 37% and X_S^L = 47% while at WHSV = 2.4 h^{-1} these values decreased to 12%, 10% and 2% respectively. The H_2 yield also diminished with space velocity as illustrated in Fig. 6. The maximum H_2 yield (31%) was obtained on Pt(2.77)/Al_2O_3 at WHSV = 0.6 h^{-1}; this η_{H_2} value is higher than those reported in bibliography for Pt-based catalysts at similar space velocities [16]. Nevertheless, from an industrial and economical point of view, the parameter to be considered to evaluate the process ability for producing hydrogen is the productivity, Pr (mol H_2/g_{cat} h), that is expressed as:

$$Pr = \frac{F_{H_2}}{W_{cat}} = \eta_{H_2}\ WHSV\ \frac{13}{M_S} \qquad (6)$$

where M_S is the molecular weight of sorbitol. The plots of Pr as a function of WHSV are presented in Fig. 7 and show that the H_2 productivity increases with Pt loading. On the four Pt catalysts, the plots of H_2 productivity went through a maximum at WHSV = 1.8 h^{-1}. The possible existence of a maximum of H_2 productivity when WHSV is increased is actually inferred from Eq.(6), because Pr increases but η_{H_2} decreases with WHSV as shown in Fig. 6. The maximum H_2 productivity (22 mmol H_2/g_{cat} h) was obtained on Pt(2.77)/Al_2O_3 at WHSV = 1.8 h^{-1}. Few papers have reported data on H_2 productivities for APR of sorbitol on Pt-based catalysts. Cortright et al. [1] obtained a value of 6 mmol H_2/g_{cat} h for H_2 production on Pt(3%)/Al_2O_3, at 498 K and 10% sorbitol in the feed. Kirilin et al. reported H_2

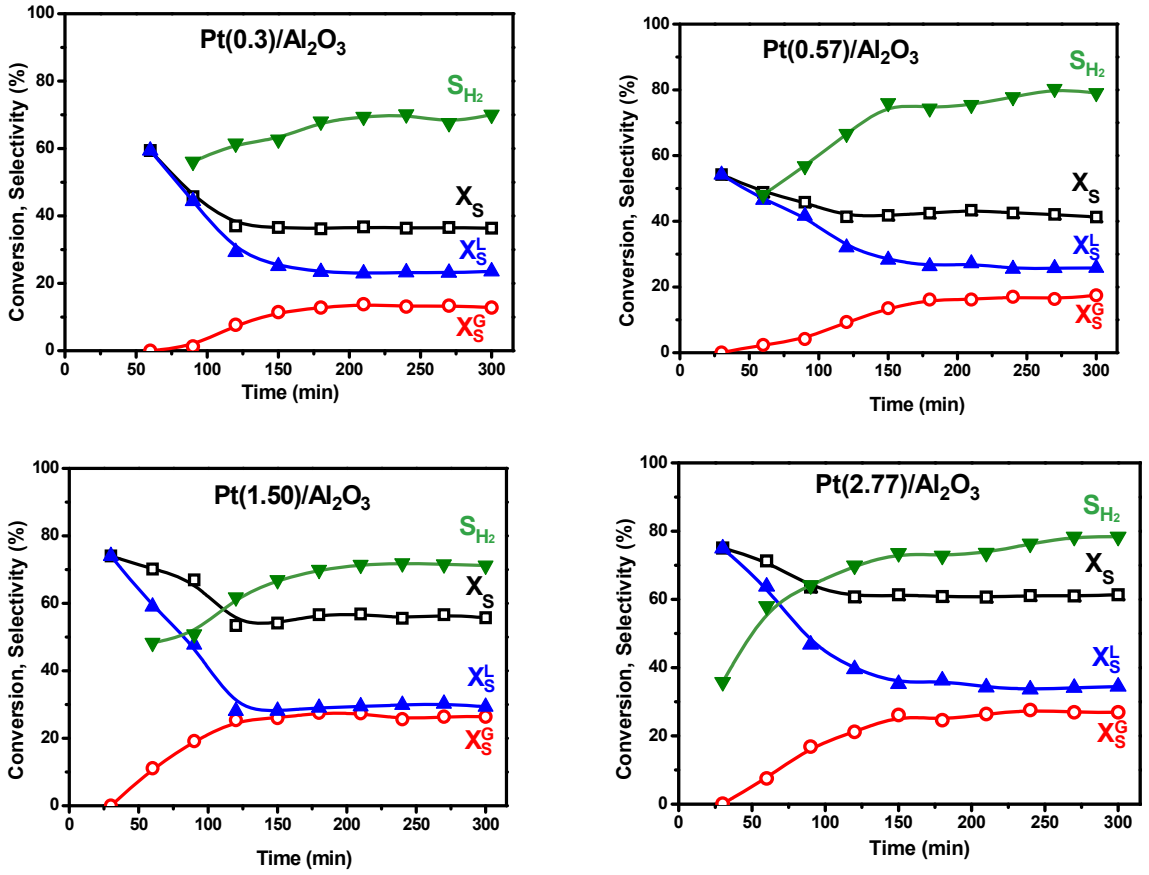

Fig. 4 – Sorbitol conversions (X_S, X_S^G, X_S^L) and H_2 selectivity (S_{H_2}) as function of time [T = 498 K; P = 29.3 bar; WHSV = 1.2 h^{-1}, W_{cat} = 0.1 g; Feed: sorbitol (1.0%)/water].

Table 2 – Catalytic results for the APR of sorbitol.

Catalyst	WHSV = 0.6 h^{-1}					WHSV = 1.2 h^{-1}					WHSV = 1.8 h^{-1}					WHSV = 2.4 h^{-1}				
	X_S	X_S^G	X_S^L	η_{H_2}	S_{H_2}	X_S	X_S^G	X_S^L	η_{H_2}	S_{H_2}	X_S	X_S^G	X_S^L	η_{H_2}	S_{H_2}	X_S	X_S^G	X_S^L	η_{H_2}	S_{H_2}
Pt(0.30)/Al_2O_3	80	21	59	18	86	36	12	24	8	70	24	9	15	6	71	6	5	1	4	82
Pt(0.57)/Al_2O_3	82	30	52	22	70	43	17	26	14	76	33	13	20	10	80	10	8	2	7	98
Pt(1.50)/Al_2O_3	84	37	47	30	81	56	26	31	19	72	38	15	23	13	86	12	10	2	9	99
Pt(2.77)/Al_2O_3	90	39	51	31	80	61	27	34	21	78	39	19	20	17	92	16	12	4	11	89

Results obtained at the end of catalytic runs. All the values are in %.
[T = 498 K; P = 29.3 bar; W_{cat} = 0.1 g; Feed: sorbitol(1.0%)/water].

productivities of 18 mmol H_2/g_{cat} h at WHSV = 2.1 h^{-1} [16] and 15 mmol H_2/g_{cat} h at 1.5 h^{-1} [14] on Pt(5%)/Al_2O_3, at 498 K, 29 bar and 10% sorbitol. At higher temperatures (523 K) and pressures (45 atm), Kim et al. [15] yielded 40 mmol H_2/g_{cat} h at WHSV = 2 h^{-1} on Pt(7%)/carbon. Finally, the H_2 productivity reported by Tanksale et al. [11] on Pt(3%)/Al_2O_3 at 473 K, 20 bar, 10% sorbitol, and WHSV = 6.2 h^{-1} was 0.23 mmol H_2/g_{cat} h. Overall, we observe that the maximum H_2 productivity obtained in the present work on Pt(2.77)/Al_2O_3 compare favorably with those reported in previous work on Pt-based catalysts.

In order to stablish the effect of sorbitol concentration on H_2 productivity, we performed additional catalytic runs of APR of sorbitol on Pt(2.77)/Al_2O_3 using sorbitol/water feeds containing 1.0, 3.3 and 5.0% sorbitol. Results obtained at WHSV = 1.2 h^{-1} are presented in Table 4. Total conversion of sorbitol increased with sorbitol concentration, from 61% (1.0% sorbitol) to 91% (5.0% sorbitol), reflecting essentially the increase of sorbitol conversion to liquid products. In contrast, X_S^G and S_{H_2}, and as a consequence the H_2 yield and productivity, did not change significantly with sorbitol concentration in the feed. This later result shows that, at a given space velocity, the H_2 productivity does not increase on Pt/Al_2O_3 catalysts by increasing the sorbitol concentration.

Finally, we investigated the effect of Pt loading on coke formation. We determined by temperature-programmed oxidation technique the amount of carbon formed on Pt/Al_2O_3 catalysts recovered from the catalytic runs of Fig. 4 that were performed at WHSV = 1.2 h^{-1} during 300 min. Before the TPO characterization, samples were treated at 523 K in N_2

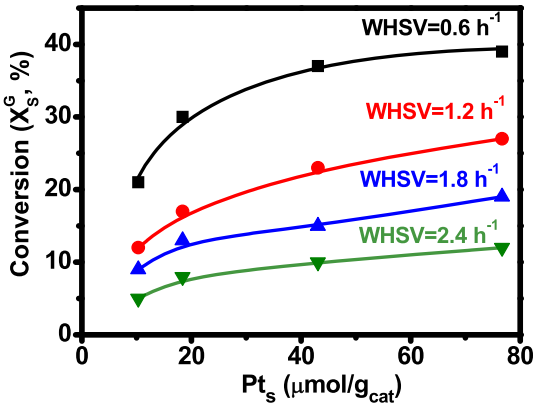

Fig. 5 – Sorbitol conversion to gaseous products (X_S^G) as a function of surface Pt fraction (Pt_s) [T = 498 K; P = 29.3 bar; W_{cat} = 0.1 g; Feed: sorbitol (1.0%)/water].

Table 3 – APR of sorbitol: Product distribution in the gas phase.

WHSV (h^{-1})	Gas composition (%, molar)							
	$Pt(0.30)/Al_2O_3$				$Pt(2.77)/Al_2O_3$			
	H_2	CO	CH_4	CO_2	H_2	CO	CH_4	CO_2
0.6	63.9	0.4	5.2	30.5	69.4	0.1	3.2	27.3
1.2	60.9	0.6	4.0	34.4	61.8	0.2	3.2	34.8
1.8	60.5	0.2	4.7	34.7	60.1	0.7	3.8	35.5
2.4	63.8	0.2	5.2	30.8	67.1	0.1	3.8	29.0

Results obtained at the end of catalytic runs.
[T = 498 K; P = 29.3 bar; W_{cat} = 0.1 g; Feed: sorbitol(1.0%)/water].

during 60 min. The obtained TPO profiles are presented in Fig. 8. The shapes of TPO curves were similar for all the samples, presenting a small peak with a maximum at about 400 K and a broad combustion band between 500 and 800 K. From the areas under the curves of Fig. 8 we determined the following carbon contents: 0.67%C [$Pt(0.30)/Al_2O_3$], 0.92%C [$Pt(0.57)/Al_2O_3$)], 0.89%C [$Pt(1.50)/Al_2O_3$] and 0.96%C [$Pt(2.77)/Al_2O_3$]. Moreover, we performed two additional catalytic tests of 48 h using $Pt(0.30)/Al_2O_3$ and $Pt(2.77)/Al_2O_3$, respectively, under the same reaction conditions of Fig. 4; we did not observe any noticeable sorbitol conversion decay during the progress of both catalytic runs. All these results showed that both the initial coke formation and catalyst deactivation do not depend significantly on Pt loading.

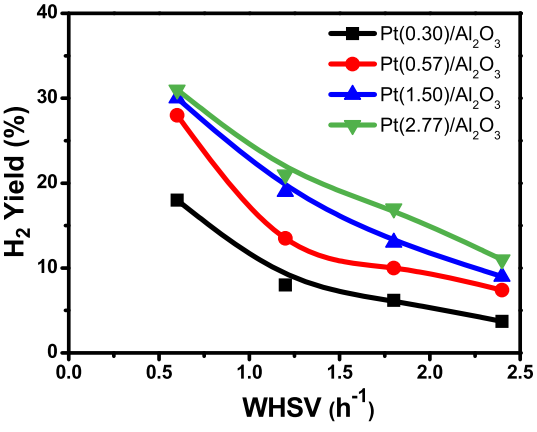

Fig. 6 – H_2 yield as a function of space velocity [T = 498 K; P = 29.3 bar; W_{cat} = 0.1 g; Feed: sorbitol (1%)/water].

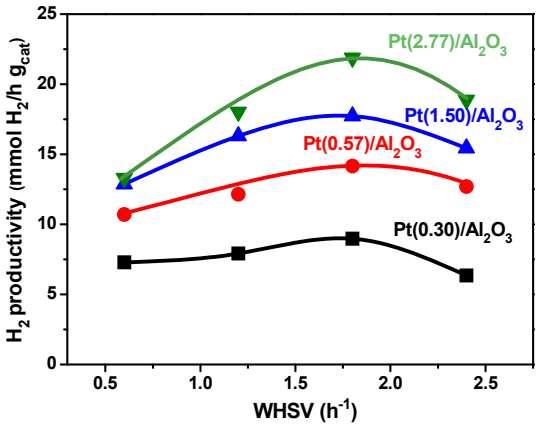

Fig. 7 – H_2 productivity as a function of space velocity [T = 498 K; P = 29.3 bar; W_{cat} = 0.1 g; Feed: sorbitol (1.0%)/water].

Table 4 – APR of sorbitol: Effect of % sorbitol.

% Sorbitol in the feed	X_S (%)	X_S^G (%)	X_S^L (%)	S_{H_2} (%)	η_{H_2} (%)	H_2 productivity (mmol H_2/h g_{cat})
1.0	61	27	34	74	21.0	18.0
3.3	85	28	57	73	21.0	18.0
5.0	91	26	65	77	20.5	17.6

Results obtained at the end of catalytic runs.
[Catalyst: $Pt(2.77)/Al_2O_3$, WHSV = 1.2 h^{-1}: T = 498 K; P = 29.3 bar; W_{cat} = 0.1 g].

Conclusions

The activity of Pt/Al_2O_3 catalysts for the aqueous-phase reforming of sorbitol depends on Pt loading. The sorbitol conversion to gaseous and liquid products increases

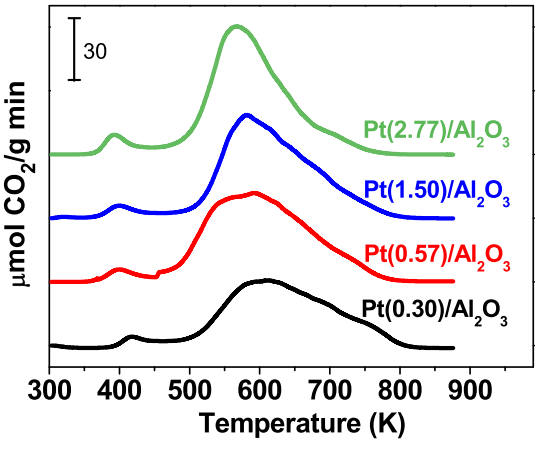

Fig. 8 – TPO profiles of Pt/Al_2O_3 samples recovered from the catalytic runs showed in Fig. 4. Heating rate, 10 K/min.

continuously, but not linearly, with the number of surface Pt atoms that in turn increases with the amount of Pt on the catalyst. Similarly, the H_2 yield increases with Pt loading; in this work, we report a maximum H_2 yield of 31%, obtained at 489 K on Pt(2.77%)/Al_2O_3 at WHSV = 0.6 h^{-1}. In contrast, the H_2 selectivity in the gas phase does not depend significantly on the amount of Pt on the catalyst. The product distribution in the gas phase was 60–70% H_2, 27–36% CO_2, 3–5% CH_4, and traces of CO, irrespective of increasing the % Pt from 0.30% to 2.77% and the space velocity from 0.6 to 2.4 h^{-1}.

The H_2 productivity increases with the amount of Pt and goes through a maximum as the space velocity is increased. Here, we obtained a maximum H_2 productivity of 22 mmol/g_{cat} h on Pt(2.77%)/Al_2O_3 at WHSV = 1.8 h^{-1}. Regarding the effect of % Pt on coke formation, we determined similar amounts of carbon deposits on the samples after the catalytic runs when the Pt loading was varied from 0.30% to 2.77%. Finally, at a given space velocity, the sorbitol conversion to liquid products increases with sorbitol concentration in the sorbitol/water reactant mixture; in contrast, the sorbitol conversion to gas products and the H_2 yield and productivity do not change significantly with the concentration of sorbitol feedstock.

Acknowledgments

Authors thank the Universidad Nacional del Litoral, Consejo Nacional de Investigaciones Científicas y Técnicas, and Agencia Nacional de Promoción Científica y Tecnológica, Argentina, for the financial support of this work.

REFERENCES

[1] Cortright RD, Davda RR, Dumesic JA. Hydrogen from catalytic reforming of biomass-derived hydrocarbons in liquid water. Nature 2002;418:964–7.
[2] Shabaker JW, Davda RR, Huber GW, Cortright RD, Dumesic JA. Aqueous-phase reforming of methanol and ethylene glycol over alumina-supported platinum catalysts. J Catal 2003;215:344–52.
[3] Shabaker JW, Dumesic JA. Kinetics of aqueous-phase reforming of oxygenated hydrocarbons: Pt/Al_2O_3 and Sn-modified Ni catalysts. Ind Eng Chem Res 2004;43:3105–12.
[4] Chheda JN, Huber GW, Dumesic JA. Liquid-phase catalytic processing of biomass-derived oxygenated hydrocarbons to fuels and chemicals. Angew Chem Int Ed 2007;46:7164–83.
[5] Tanksale A, Wong Y, Beltramini JN, Lu GQ. Hydrogen generation from liquid phase catalytic reforming of sugar solutions using metal-supported catalysts. Int J Hydrogen Energy 2007;32:717–24.
[6] Davda RR, Shabaker JW, Huber GW, Cortright RD, Dumesic JA. A review of catalytic issues and process conditions for renewable hydrogen and alkanes by aqueous-phase reforming of oxygenated hydrocarbons over supported metal catalysts. Appl Catal B Environ 2005;56:171–86.
[7] Huber GW, Shabaker JW, Evans ST, Dumesic JA. Aqueous-phase reforming of ethylene glycol over supported Pt and Pd bimetallic catalysts. Appl Catal B Environ 2006;62:226–35.
[8] Shabaker JW, Huber GW, Davda RR, Cortright RD, Dumesic JA. Aqueous-Phase Reforming of ethylene glycol over supported platinum catalysts. Catal Lett 2003;88:1–8.
[9] Lehnert K, Claus P. Influence of Pt particle size and support type on the aqueous-phase reforming of glycerol. Catal Commun 2008;9:2543–6.
[10] Wawrzetz A, Peng B, Hrabar A, Jentys A, Lemonidou AA, Lercher JA. Towards understanding the bifunctional hydrodeoxygenation and aqueous phase reforming of glycerol. J Catal 2010;269:411–20.
[11] Tanksale A, Beltramini JN, Dumesic JA, Lu GQ. Effect of Pt and Pd promoter on Ni supported catalysts. A TPR/TPO/TPD and microcalorimetry study. J Catal 2008;258:366–77.
[12] Kirilin AV, Tokarev AV, Murzina EV, Kustov LM, Mikkola JP, Murzin DYu. Reaction products and transformations of intermediates in the aqueous-phase reforming of sorbitol. ChemSusChem 2010;3:708–18.
[13] Aiouachea F, McAleerb L, Ganb Q, Al-Muhtasebc AH, Ahmadb MN. Path lumping kinetic model for aqueous phase reforming of sorbitol. Appl Catal A General 2013;466:240–55.
[14] Kirilin AV, Wärna J, Tokarev AV, Murzin DYu. Kinetic modeling of sorbitol aqueous-phase reforming over Pt/Al_2O_3. Ind Eng Chem Res 2014;53:4580–8.
[15] Kim TW, Kim MC, Yang YC, Kim YR, Jeong SY, Kim CU. Hydrogen production via the aqueous phase reforming of polyols over CMK-9 mesoporous carbon supported platinum catalysts. Int J Hydrogen Energy 2015;40:15236–43.
[16] Kirilin AV, Tokarev AV, Kustov LM, Salmi T, Mikkola JP, Murzin DYu. Aqueous phase reforming of xylitol and sorbitol: comparison and influence of substrate structure. Appl Catal A General 2012;435–436:172–80.
[17] Li N, Huber GW. Aqueous-phase hydrodeoxygenation of sorbitol with Pt/SiO_2-Al_2O_3: identification of reaction intermediates. J Catal 2010;270:48–59.
[18] Neira D'Angelo MF, Ordomsky V, van der Schaaf J, Schouten JC, Nijhuis TA. Aqueous phase reforming in a microchannel reactor: the effect of mass transfer on hydrogen selectivity. Catal Sci Technol 2013;3:2834–42.
[19] Davda RR, Shabaker JW, Huber GW, Cortright RD, Dumesic JA. Aqueous-phase reforming of ethylene glycol on silica-supported metal catalysts. Appl Catal B Environ 2003;43:13–26.
[20] Huber GW, Cortright RD, Dumesic JA. Renewable alkanes by aqueous-phase reforming of biomass-derived oxygenates. Angew Chem Int Ed 2004;43:1549–51.
[21] Borgna A, Garetto TF, Apesteguia CR, Le Normand F, Moraweck B. Sintering of chlorinated Pt/γ-Al_2O_3 catalysts: an in-situ study by X-ray absorption spectroscopy. J Catal 1999;86:433–41.
[22] Garetto TF, Rincón E, Apesteguía CR. The origin of the enhanced activity of Pt/zeolites for combustion of C_2-C_4 alkanes. Appl Catal B Environ 2007;73:65–72.
[23] Bertero NM, Trasarti AF, Apesteguía CR, Marchi AJ. Liquid-phase dehydration of 1-phenylethanol on acid solids: influence of catalyst acidity and pore structure. Appl Catal A General 2013;458:28–38.